Open Journal of Mathematical Sciences

PSR Press

Article

Diversified role of brownian motion and thermophoresis on time-dependent stagnation-point flow of nanofluid over a stretching surface with chemical reaction

Moon Das* **and S. N. Mohapatra**

Department of Mathematics, Bhattadev University, Assam, 781325, India

* Correspondence: way2moondas@gmail.com

Received: 04 Jun 2025; Revised: 11 Jan 2026; Accepted: 03 Feb 2026; Published: 17 May 2026

Abstract: The enhanced thermal performance of nanofluids is highly important for improving heat transfer performance in diversified engineering applications. Furthermore, the interaction of chemical reactions is important in biomedical applications such as targeted therapy, drug delivery, and related processes. The present investigation aims to study the time-dependent stagnation-point flow of a two-phase model nanofluid along a stretching surface, emphasizing the diversified roles of Brownian motion vis-à-vis thermophoresis in the presence of chemical species. Moreover, the conducting fluid flowing through a porous medium affects the flow phenomena with the simultaneous involvement of thermal radiation and a heat source. The proposed mathematical model, originally expressed in dimensional form, is transformed into a non-dimensional form through the introduction of suitable similarity rules, and the resulting transformed set of equations is handled numerically. In particular, a numerical technique based on the fourth-order Runge–Kutta method is employed for the solution of the transformed equations. The physical significance of several parameters associated with the flow phenomena is presented graphically and discussed briefly. The key findings include the roles of Brownian motion and thermophoresis in enhancing nanoparticle transport, which improves thermal efficiency. The magnetization effect, together with the porous medium, plays a critical role in controlling the flow and thermal characteristics.

Keywords: nanofluid heat transfer, stagnation-point flow, Brownian motion, thermophoresis, chemical reaction

MSC: 76W05, 80A20

1. Introduction

In recent years, nanofluids [1] have gained considerable attention from researchers because of their remarkable heat transfer enhancement characteristics. The integration of nanoparticles into base fluids improves the heat transfer rate of coolants and strengthens their thermal performance. Various heat transfer applications, including renewable energy systems, are crucial for addressing the global energy crisis. Nanofluids, introduced by Choi, represent a significant advancement in fluid dynamics because they enhance the thermal engineering properties of conventional fluids and exhibit vast potential in diverse fields such as medical engineering and energy engineering. Nanofluids also enhance targeted drug delivery as therapeutic agents by increasing efficiency and reducing possible side effects. Furthermore, they are used in cancer treatments, where they improve heat dissipation and provide more precise temperature control within the tumour region. Moreover, nanofluids containing magnetic nanoparticles are applied in advanced imaging techniques, such as magnetic resonance imaging. In several electronic components, nanofluids play an important role as coolants for avoiding overheating. They are also useful in enhancing engine cooling systems and improving lubrication properties, which ultimately contributes to increased vehicle efficiency.

Researchers have found that suspending tiny solid particles within traditional fluids increases absorption in efficient solar collectors [2]. Additionally, these particles suspended in water can be treated as more effective coolants for industrial requirements, leading to enhanced economy and improved safety [3]. Furthermore,

nanofluids are utilized to improve heat exchange performance by reducing internal heat accumulation. They find applications in hybrid power engines, transformer oil cooling, improved chiller and refrigerator efficiency, and diesel engine oil cooling [4]. Ferrofluids, which are composed of ferromagnetic nanoparticles of approximately 10 nm suspended in a liquid, are also crucial. Recent studies have demonstrated their applicability in biomedicine, including hyperthermia treatment, targeted drug delivery, cell separation, and imaging [5,6]. Nanofluids have penetrated various biomedical applications by offering biologically friendly, sustainable, and durable solutions. Despite significant experimental efforts, theoretical and computational investigations have further advanced nanofluid research. However, several studies have considered the flow of magnetic-particle-based fluids in mechanical systems by examining either time-dependent, time-independent, or other related configurations. Turkyilmazoglu [7] presented the circulation of nanomaterial over a rotating disk, and the corresponding flow model was solved by utilizing the spectral Chebyshev collocation method. In that study, various nanoparticles were dispersed in a Newtonian fluid, namely water, with copper nanofluids exhibiting an optimal rate of energy transport. Furthermore, Hayat and co-workers [8] introduced the homotopy technique to explore chemical reactions in magnetite-Fe_3O_4 nanofluid under the influence of a magnetic field.

Following Sheikholeslami's pioneering work [9], numerous researchers have investigated several physical aspects, such as suction/blowing, magnetic fields, and thermal radiation. Magnetohydrodynamic interaction in various fluids, particularly in the presence or absence of a porous substance, has attracted significant interest because of its diversified engineering applications. Sheikholeslami [10,11] investigated the flow characteristics of different solid nanoparticles embedded within a permeable matrix while considering the roles of magnetization and electric field. Similarly, Gorla and Chamkha [12,13] proposed the flow phenomena of a non-Newtonian nanomaterial with the interaction of thermal buoyancy through a saturated porous substance. Chamkha et al. [14,15] further reported the flow of a non-Newtonian fluid enforced by the role of an electrically conducting medium affecting the physical properties in the presence of a porous matrix. Bég et al. [16] investigated the role of expanding and contracting flow dynamics in bioconvection nanofluid within a deformable channel. Their findings indicated that gyrotactic microorganisms present in the base liquid, together with the interaction of solid particles, significantly overshoot the mass flux at the wall for both nanofluid and microorganisms. Li et al. [17] conducted a numerical analysis by adopting a time-dependent bioconvection nanofluid model within two rotating discs. Their investigation was based on mixed convective flow with the interaction of several characterizing parameters. Furthermore, several analyses have been carried out by considering nanomaterial swirl flow within a rotating disc by Imtiaz et al. [18] and Hayat et al. [19], who explored scenarios involving carbon nanotubes and magnetite-Fe_3O_4 ferro-nanofluid, respectively. Earlier, Bég et al. [20] presented an analysis of irreversibility processes within the system due to the energy transport properties of magnetized swirl flow past an extending rotating disk. In a novel approach, Hayat et al. [21] proposed variable properties for the thickness of a rotating disc by considering the Von Kármán swirl motion with the impact of radiating energy. Karimipour et al. [22–24] reported gravity effects on mixed convection heat transfer, focusing on the inclined magnetic field, and a robust lattice Boltzmann method was utilized to handle the proposed flow phenomena. Recently, Chamkha and Aly [25] considered flow through a vertical plate for the proposed nanoparticles while presenting the behavior of the external heat source applied to it. Biglarian et al. [26] and Rahimi et al. [27] conducted investigations on squeezing nanofluid heat transfer, respectively. Baag and Mishra [28] recently investigated magnetized three-dimensional H_2O-based nanofluid, while Makinde and Mishra [29] explored the circulation of variable-viscosity nanofluids along a stretching surface with radiating energy. Additionally, Das et al. [30] presented the role of radiating heat on nanomaterial flow over a transient stretching surface. Researchers [31–33] have also reported nanomaterial flow with different effective effects along an elastic surface. Li et al. [34–37] explored the mechanism by considering the impact of wall properties and variable liquid characteristics. Sulochana et al. [38] studied the impact of multi-walled carbon nanotubes (MWCNTs) and hybrid biodiesel blends on the performance, combustion, and emission characteristics of a compression ignition engine. Li et al. [39–41] considered the combined effects of linear thermal radiation and chemical reactions on heat and mass transfer behavior. Their investigation was also conducted under convective mass and thermal boundary conditions. The novel physical effects of key parameters were examined and presented graphically. Researchers [42,43] studied the flow of viscous liquid over a stretching surface. Shamshuddin et al. [44] examined two-phase micropolar nanofluid flow over an isothermal extending porous sheet, highlighting the combined influences of heat radiation and

chemical interaction. Similarly, Swapna et al. [45] explored the nonorthogonal stagnation-point flow of micropolar fluids past a stretching sheet, emphasizing the effects of thermal radiation and chemical reactions on heat transfer behavior. Furthermore, the complex dissipative and radiative characteristics of micropolar hybrid nanofluid flow over a wedged geometry were numerically investigated by Shamshuddin et al. [46] using a Gauss–Lobatto IIIA scheme. The interplay of ferromagnetic forces, ohmic heating, and nanoparticle size variation in a rotating disk nanofluid system was also analyzed by Shamshuddin et al. [47], revealing significant changes in radial transport mechanisms. Moreover, unsteady convective hydromagnetic flow with chemical reactions, dissipation, and radiation in an inclined porous medium was addressed by Sademaki et al. [48], providing insight into the thermal migration of reactive species.

1.1. Motivation and objectives of the study

The motivation and objectives of the present study are summarized as follows:

- Studying heat transport properties in fluids with chemical reactions on stretching sheets is significant in diversified sectors, particularly in chemical engineering, and it has an important impact on fields such as food processing, polymer production, and related industrial applications.
- Coupled energy and mass transfer models, especially those involving chemical species, are vital across various physical and engineering processes and have received considerable attention in recent investigations.
- Earlier studies on this diversified topic motivated the present exploration of the role of cross-diffusion effects on the time-dependent stagnation-point nanofluidic motion along a stretching surface.
- The impact of radiating energy on a conducting fluid, together with the involvement of heat source/sink and chemical reaction, enriches the flow phenomena significantly.
- The main objective is to develop a comprehensive study of the influence of various factors affecting the heat transfer phenomena and associated transport characteristics.

The present study provides a novel approach through the integrated analysis of Brownian motion and thermophoresis in a time-dependent nanofluid flow with the impact of magnetic field, porosity, thermal radiation, heat source, and chemical reaction. Efficient numerical accuracy is obtained by utilizing a shooting-based Runge–Kutta technique implemented through MATLAB software.

2. Mathematical formulation

This section provides the mathematical formulation of the problem, including the governing equations in both dimensional and non-dimensional forms. The boundary conditions and relevant physical parameters are defined, thereby laying the foundation for subsequent analyses. A two-phase nanofluid flow is considered, where the role of cross-diffusion effects in a conducting fluid over a stretching surface embedded in a permeable medium is examined. The model exhibits the interaction of random particle motion caused by Brownian diffusion and the thermal-gradient-driven migration due to thermophoresis. In addition, the effects of a heat source and chemical reaction enrich the flow properties. The flow is assumed to take place along the x-direction, whereas the normal direction is treated as the y-direction and is confined to the positive region. The assumption indicates that, at $t = 0$, the flow of the fluid is considered steady; otherwise,

$$U_w(x,t) = \frac{ax}{1-\lambda t}$$

is proposed as the time-dependent velocity along the x-axis. In particular,

$$U_e(x,t) = \frac{bx}{1-\lambda t}$$

is considered as the velocity of the fluid far away from the sheet. Here, the constants a and b are termed the stretching rate and stagnation-flow rate, respectively, with dimension time^{-1}, while λ is the rate constant with dimension time^{-1}. Similarly,

$$T_w(x,t) = T_\infty + T_0\left[\frac{ax^2}{(1-\lambda t)^{-2}}\right],$$

and

$$C_w(x,t) = C_\infty + C_0\left[\frac{ax^2}{(1-\lambda t)^{-2}}\right]$$

are assumed to be the plate temperature and concentration of the sheet, respectively. In particular, the positive constants T_0 and C_0, with $0 \leq T_0 \leq T_w$ and $0 \leq C_0 \leq C_w$, are introduced as the reference temperature and concentration, respectively. Furthermore, the radiative heat impact through the role of heat flux is assumed, leading to the influence of radiating energy on the heat transfer flow phenomena.

The flow configuration is shown in Figure 1.

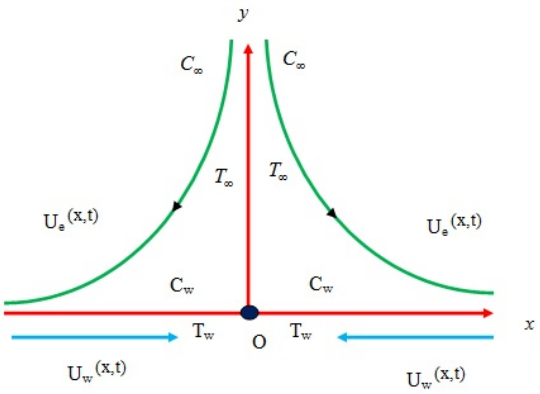

Figure 1. Flow configuration of the proposed physical model

In particular, the following assumptions are made in the proposed problem:

- A time-dependent two-phase flow of nanofluid is considered.
- The flow over a stretching sheet embedded in a porous matrix is proposed.
- The assumptions of Brownian motion and thermophoresis are vital for the nanoparticle transport mechanism.
- The inclusion of heat source, thermal radiation, and chemical reaction is important for enriching the physical model.
- The surface temperature and concentration are considered to be variable.

The mathematical model designed for the aforementioned assumptions, following Das et al. [30], together with the appropriate surface conditions, is given as follows:

$$\frac{\partial u}{\partial x} + \frac{\partial v}{\partial y} = 0, \tag{1}$$

$$\frac{\partial u}{\partial t} + u\frac{\partial u}{\partial x} + v\frac{\partial u}{\partial y} = \frac{\partial U_e}{\partial t} + U_e\frac{\partial U_e}{\partial x} + \nu_f\frac{\partial^2 u}{\partial y^2} - \frac{\sigma B_0^2}{\rho_f}(u-U_e) - \frac{\nu_f}{Kp}(u-U_e), \tag{2}$$

$$\frac{\partial T}{\partial t} + u\frac{\partial T}{\partial x} + v\frac{\partial T}{\partial y} = \alpha\frac{\partial^2 T}{\partial y^2} + \tau\left[D_B\frac{\partial T}{\partial y}\frac{\partial C}{\partial y} + \left(\frac{D_e}{T_\infty}\right)\left(\frac{\partial T}{\partial y}\right)^2\right] - \frac{1}{(\rho c)_f}\frac{\partial q_r}{\partial y} + \frac{Q}{(\rho c)_f}(T-T_\infty), \tag{3}$$

$$\frac{\partial C}{\partial t} + u\frac{\partial C}{\partial x} + v\frac{\partial C}{\partial y} = D_B\frac{\partial^2 C}{\partial y^2} + \left(\frac{D_T}{T_\infty}\right)\frac{\partial^2 T}{\partial y^2} - Kc(C-C_\infty). \tag{4}$$

The related boundary constraints are

$$\text{At } y=0: \begin{cases} v=0, \quad u=U_w(x,t), \\ T=T_w(x,t), \\ C=C_w(x,t), \end{cases} \qquad \text{as } y\to\infty: \begin{cases} u\to U_e(x,t), \\ T\to T_\infty, \\ C\to C_\infty. \end{cases} \tag{5}$$

The proposed set of equations related to the flow phenomena is presented in the Cartesian coordinate system with flow directions (x,y) and corresponding velocity components (u,v). Also, B_0 denotes the

strength of the uniform magnetic field applied along the normal direction of the flow, while Kp represents the permeability of the porous medium. Moreover,

$$\alpha = \frac{\kappa}{(\rho c)_f}, \quad \text{thermal diffusivity,} \qquad \tau = \frac{(\rho c)_s}{(\rho c)_f}, \quad \text{specific heat capacity ratio,}$$

and other physical quantities are defined according to the standard nanofluid model.

The interaction of nonlinear heat flux under the Rosseland approximation is expressed in the standard form as

$$q_r = -\frac{4\sigma^*}{3k^*}\frac{\partial T^4}{\partial y}. \tag{6}$$

In general, σ^* denotes the Stefan–Boltzmann constant, and k^* denotes the mean absorption coefficient.

Linearizing T^4 about T_∞, following Das et al. [30], yields

$$T^4 = 4T_\infty^3 T - 3T_\infty^4. \tag{7}$$

The radiative heat flux presented in Eq. (6) can therefore be modified as

$$q_r = -\frac{16T_\infty^3\sigma^*}{3k^*}\frac{\partial T}{\partial y}, \qquad \frac{\partial q_r}{\partial y} = -\frac{16T_\infty^3\sigma^*}{3k^*}\frac{\partial^2 T}{\partial y^2}. \tag{8}$$

Using Eq. (8) in Eq. (3) leads to

$$\frac{\partial T}{\partial t} + u\frac{\partial T}{\partial x} + v\frac{\partial T}{\partial y} = \alpha\left(1 + \frac{16T_\infty^3\sigma^*}{3k^*\kappa}\right)\frac{\partial^2 T}{\partial y^2} + \tau\left[D_B\frac{\partial T}{\partial y}\frac{\partial C}{\partial y} + \left(\frac{D_e}{T_\infty}\right)\left(\frac{\partial T}{\partial y}\right)^2\right] + \frac{(T-T_\infty)Q}{(\rho c)_f}. \tag{9}$$

The contribution of Brownian motion enhances the energy exchange between nanoparticles and the base fluid, which gives rise to the effective thermal conductivity of the nanofluid. It facilitates the distribution of energy and plays a critical role in the convective heat transfer properties. Moreover, it leads to a more uniform nanoparticle distribution. Thermophoresis, on the other hand, causes nanoparticles to migrate from hotter regions to cooler regions. This phenomenon modifies the thermal boundary layer and consequently influences the heat transfer rates.

2.1. Similarity rules

The proposed model, designed through the governing Eqs. (1)–(5) and Eq. (7), is initially expressed in dimensional form. Therefore, suitable transformation rules are required to convert the system into a standard non-dimensional form.

$$\left.\begin{aligned} \eta(y,t) &= \sqrt{\frac{a}{\nu_f(1-\lambda t)}}\, y, \\ \psi(x,y,t) &= \sqrt{\frac{a\nu_f}{1-\lambda t}}\, x f(\eta), \\ T &= T_\infty + T_0\left[\frac{ax^2}{(1-\lambda t)^{-2}}\right]\theta(\eta), \\ C &= C_\infty + C_0\left[\frac{ax^2}{(1-\lambda t)^{-2}}\right]\phi(\eta). \end{aligned}\right\} \tag{10}$$

The velocity components are defined as

$$u = \frac{\partial \psi}{\partial y}, \qquad v = -\frac{\partial \psi}{\partial x},$$

which satisfy the continuity Eq. (1) through the stream function ψ. These quantities are defined as

$$u = \left(\frac{ax}{1-\lambda t}\right) f'(\eta), \qquad v = -\sqrt{\frac{av_f}{1-\lambda t}}\, f(\eta), \qquad T = T_\infty + (T_w - T_\infty)\theta(\eta), \qquad C = C_\infty + (C_w - C_\infty)\phi(\eta). \tag{11}$$

Now, implementing Eqs. (10) and (11) into the flow equations, namely Eq. (2), together with Eq. (4) and Eq. (9), and applying the surface condition Eq. (5), leads to

$$f''' + f''\left(f - \frac{1}{2}\eta S\right) - f'(f' + S) + \beta^2 + \beta S - (M + Da)f' = 0, \tag{12}$$

$$\frac{1}{Pr}(1 + Nr)\theta'' + S\left(2\theta - \frac{1}{2}\theta'\eta\right) + f\theta' - 2f'\theta + Nb\,\theta'\phi' + Nt\,\theta'^2 + H\theta = 0, \tag{13}$$

$$\frac{1}{Le\,Pr}\phi'' - S\left(\frac{1}{2}\eta\phi' - 2\phi\right) - 2f'\phi + f\phi' + \frac{Nt}{Le\,Pr\,Nb}\theta'' - \gamma\phi = 0, \tag{14}$$

$$\left.\begin{aligned} &f'(0) = 1, \quad f(0) = 0, \quad \theta(0) = 1, \quad \phi(0) = 1, \quad \text{at } \eta = 0, \\ &f'(\eta) = 0, \quad \theta(\eta) = 0, \quad \phi(\eta) = 0, \quad \text{as } \eta \to \infty. \end{aligned}\right\} \tag{15}$$

Here, $S = \frac{\lambda}{a}$ is the transient parameter, $\beta = \frac{b}{a}$ is the velocity ratio term, $M = \frac{\sigma_f B_0^2}{a\rho_f}$ is the magnetization parameter, $Da = \frac{\nu_f}{aKp}$ is the porosity parameter, $Pr = \frac{\nu_f}{\alpha_f}$ is the Prandtl number, $Nr = \frac{16T_\infty^3\sigma^*}{3k^*\kappa}$ is the thermal radiation parameter, $Nb = \frac{\tau D_B(C_w - C_\infty)}{\nu_f}$ is the Brownian motion parameter, $Nt = \frac{\tau D_T(T_w - T_\infty)}{\nu_f T_\infty}$ is the thermophoresis parameter, $\gamma = \frac{Kc}{a}$ is the chemical reaction parameter, and $Le = \frac{\alpha_f}{D_B}$ is the Lewis number.

2.2. Engineering quantities of interest

The engineering coefficients formulated for the proposed model, namely the shear rate C_f, the heat transfer rate Nu, and the solutal transfer rate Sh, are presented as follows:

$$C_f = \frac{\mu}{\rho_f U_w^2}\left(\frac{\partial u}{\partial y}\right)_{y=0}, \tag{16}$$

$$Nu = -\frac{x}{\kappa(T_w - T_\infty)}\left[\kappa\left(\frac{\partial T}{\partial y}\right)_{y=0} + \frac{4\sigma^*}{3k^*}\left(\frac{\partial T}{\partial y}\right)_{y=0}\right], \tag{17}$$

$$Sh = -\frac{x}{(C_w - C_\infty)}\left(\frac{\partial C}{\partial y}\right)_{y=0}. \tag{18}$$

Substituting the similarity transformations into Eqs. (16)–(18) gives

$$C_{fx} = Re_x^{1/2}C_f = f''(0), \qquad Nu_x = Re_x^{-1/2}Nu = -(1 + Nr)\theta'(0), \qquad Sh_x = Re_x^{-1/2}Sh = -\phi'(0),$$

where

$$Re_x = \frac{U_w x}{\nu_f}$$

denotes the local Reynolds number.

Table 1 presents the comparison of $f''(0)$ for the limiting case $M = Da = \beta = 0$. The close agreement of the present results with those reported by Ishak et al. [42] and Vajravelu et al. [43] verifies the accuracy and reliability of the numerical procedure employed in the present study.

Table 1. Comparison of $f''(0)$ for $M = Da = \beta = 0$

S	Ishak et al. [42]	Vajravelu et al. [43]	Present study
0	1.000000	1.000000	1.000484
1	1.682000	1.681921	1.681939

3. Methodology

The mathematical model proposed in this investigation, together with the associated characterizing parameters, is nonlinear and coupled. Therefore, a numerical method is a suitable approach to handle the present problem effectively. Initially, the governing higher-order system of differential equations, together with the boundary conditions, is reduced to a first-order ordinary differential system. The following transformations are introduced:

$$f = y_1, \quad f' = y_2, \quad f'' = y_3, \quad \theta = y_4, \quad \theta' = y_5, \quad \phi = y_6, \quad \phi' = y_7.$$

Thus, the transformed first-order system is written as

$$y_3' = -\left[y_3\left(y_1 - \frac{1}{2}\eta S\right) - y_2(y_2 + S) + \beta^2 + \beta S - (M + Da)y_2\right],$$

$$y_5' = -\left[S\left(2y_4 - \frac{1}{2}y_5\eta\right) + y_1y_5 - 2y_2y_4 + Nb\, y_5y_7 + Nt\, y_5^2 + Hy_4\right] \Bigg/ \left[\frac{1}{Pr}(1 + Nr)\right],$$

$$y_7' = -\left[-S\left(\frac{1}{2}\eta y_7 - 2y_6\right) - 2y_2y_6 + y_1y_7 + \frac{Nt}{Le\, Pr\, Nb}y_5' - \gamma y_6\right] \Bigg/ \left[\frac{1}{Le\, Pr}\right].$$

The transformed boundary conditions are expressed as

$$\left.\begin{array}{lll} y_a(2) = 1, \quad y_a(1) = 0, \quad y_a(4) = 1, \quad y_a(6) = 1, & & \text{at } \eta = 0, \\ y_b(2) \to 0, \quad y_b(4) \to 0, \quad y_b(6) \to 0, & & \text{as } \eta \to \infty. \end{array}\right\}$$

Here, y_a and y_b denote the values of the dependent variables at the lower and upper boundaries, respectively.

The assumed unknown initial values are obtained by employing the Newton shooting technique, and then the resulting first-order system is solved numerically by using the fourth-order Runge–Kutta technique. A step size of 0.01 is considered, and the iterative procedure is continued until an accuracy of 10^{-5} is achieved. The asymptotic behavior of the profiles confirms the convergence properties and reliability of the proposed numerical methodology.

4. Results with parametric role

The results of the study are presented and analyzed in detail in this section. The velocity field, thermal field, and concentration field are examined under various parametric influences, including magnetic field strength, external heat source, and reacting species. Graphical representations and tabulated data facilitate a comprehensive understanding of the findings. Computational analyses were conducted using MATLAB software by employing the fourth-order Runge–Kutta method together with the Newton shooting technique. The physical characteristics of diversified parameters, specifically the magnetization parameter (M), heat generation/sink parameter (H), and chemical reaction parameter (γ), along with other factors such as the unsteadiness constraint (S), stretching parameter (β), thermophoresis parameter (Nt), Brownian motion parameter (Nb), and Lewis number (Le), are presented graphically. However, the simulation process is carried out by keeping the Prandtl number (Pr) constant at 6.9 throughout the calculations.

The impact of these parameters on various engineering coefficients is also depicted through graphs and tables. The results are compared with the earlier works of Ishak et al. [42] and Vajravelu et al. [43] in a particular limiting case, and the numerical results are presented in Table 1. The comparative results show good agreement, thereby validating the present Runge–Kutta methodology against the previously reported Keller–Box method.

4.1. Velocity profiles

The fluid velocity is affected by several factors, as indicated in the governing transformed equations. Figure 2 illustrates the velocity profiles for the impact of magnetization, and the results are implemented in two different cases, namely the presence and absence of a porous matrix. The parametric variation of the magnetic term is considered within the range $0 \leq M \leq 3$. In particular, $M = 0$ signifies the absence of magnetization,

whereas nonzero values indicate the impact of the magnetic field on the flow profiles. Moreover, $Da = 0$ indicates flow through a clear fluid, while $Da = 1$ indicates flow through a porous medium.

The involvement of magnetization generally produces a resistive force. This resistive force arises due to the occurrence of the Lorentz force, which tends to oppose the fluid motion. Therefore, increasing magnetization retards the velocity profile, which results in a reduction of the velocity boundary-layer thickness. This behavior occurs in both porous and nonporous regions. However, the inclusion of permeability also acts as a resistive force and consequently decelerates the velocity distribution.

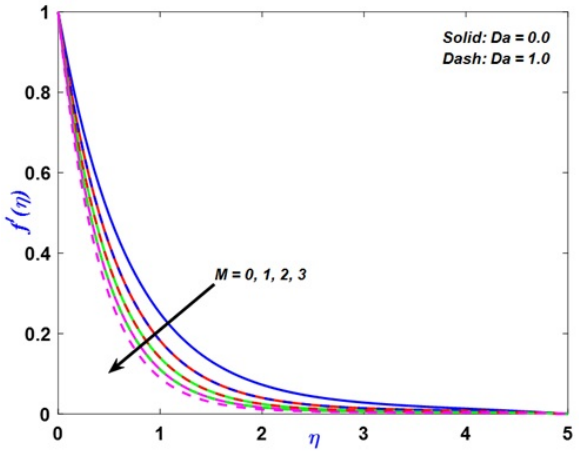

Figure 2. Impact of the magnetic parameter on the velocity profile

Figure 3 describes the behavior of the velocity ratio parameter on the velocity distribution with and without the unsteadiness term. The variation of the velocity ratio parameter is presented within the range $0.1 \leq \beta \leq 0.7$, while the numerically assigned value $S = 0$ represents the steady state and $S = 0.5$ represents the unsteady state. In the steady-state case, the results align well with previous studies, while in the unsteady-state case, agreement is also observed with published results. The graphical illustration shows that the steady-state condition is dominated by the unsteady-state condition, and the profile increases significantly with increasing values of the velocity ratio.

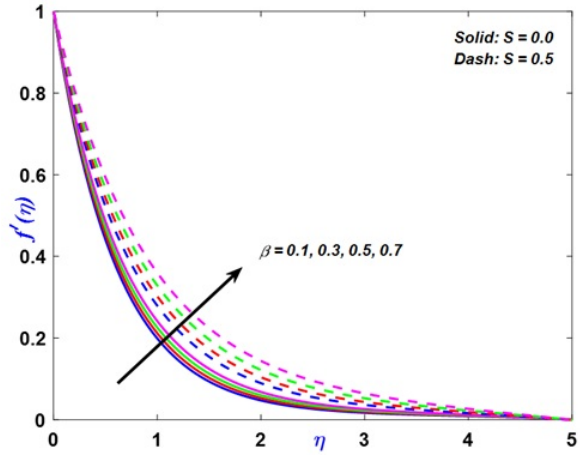

Figure 3. Impact of the stretching ratio on the velocity profile

4.2. Temperature profiles

The fluid temperature is affected by various factors involved in the heat transport phenomenon within their appropriate ranges, as presented in the governing equations. The behavior of radiating energy on the fluid temperature is presented in Figure 4 for the variation of the heat source/sink parameter. The numerical value $H = -0.1$ represents the case of heat sink, while $H = 0.1$ suggests the case of heat source. However,

when $Nr = 0$, there is no thermal radiation, and the ability to emit heat is limited, which results in a slower rise of the fluid temperature.

Furthermore, increasing radiant heat enhances the heat transport properties, and the fluid temperature is boosted effectively irrespective of the heat absorption or heat source scenario. Thermal radiation is a measure of the electromagnetic waves released from the fluid element. The emitted electromagnetic waves are further transformed into radiating heat, known as thermal radiation. This causes a significant increase in the temperature profile. Moreover, in the case of a heat sink, heat is removed from the system, whereas in the case of a heat source, additional thermal energy is supplied toward the surface. Therefore, the intensified heat source boosts the fluid temperature, while the heat sink opposes it throughout the domain. The asymptotic nature of the profile shows that the profile satisfies the far-field boundary condition and approaches zero at infinity.

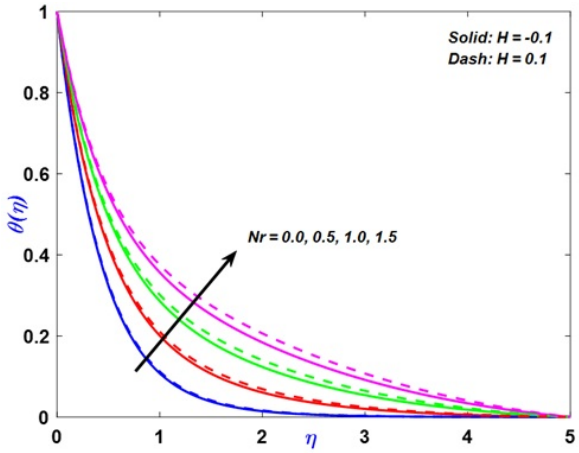

Figure 4. Role of thermal radiation on the temperature profile

The nanofluid flow phenomenon is exhibited through the interaction of cross-diffusion effects, which introduces the roles of Brownian motion and thermophoresis in the thermal field. Figures 5 and 6 elaborate the behavior of Brownian motion and thermophoresis on the thermal field, respectively. These effects are analyzed by varying their values from $Nb = 0.1$ to 0.4 and from $Nt = 0.1$ to 0.4 under both the steady-state condition $(S = 0)$ and the unsteady-state condition $(S = 0.1)$.

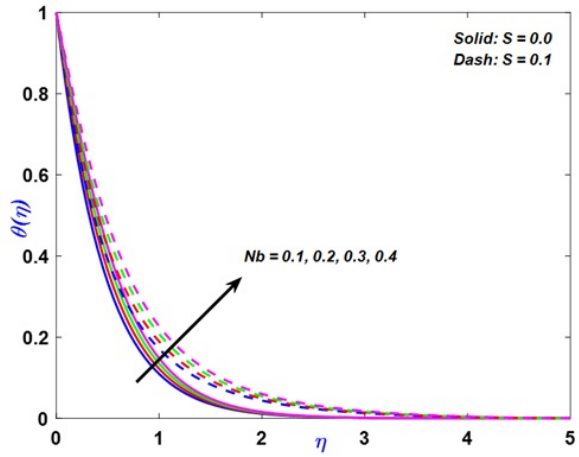

Figure 5. Role of Brownian motion on the temperature profile

In the steady state, an increase in Brownian motion within the specified range raises the thermal property. This observation is due to the enhanced random motion of nanoparticles for higher Brownian motion, which causes greater diffusion of heat. However, since Brownian motion primarily contributes to mass transfer rather

than heat transfer, its effect on temperature is moderate. Furthermore, for increasing thermophoresis within its range, the fluid temperature also experiences a significant increase. Thermophoresis drives particles from the hotter region toward the cooler region, causing a transfer of heat within the system. Therefore, higher values of Nt significantly amplify the fluid temperature. In the unsteady state, the profile is more pronounced, and the fluid temperature increases throughout the domain, dominating the steady-state condition.

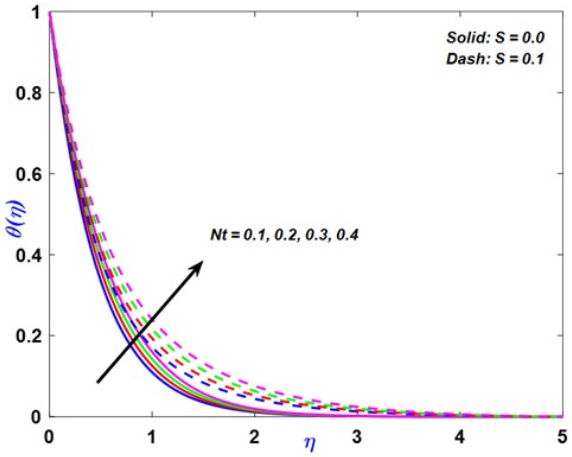

Figure 6. Role of thermophoresis on the temperature profile

4.3. Concentration profiles

The fluid concentration equation is coupled with both the flow and heat transport phenomena. Therefore, several factors also affect the concentration distribution with the involvement of the chemical reaction term. Figure 7 presents the impact of the Lewis number on the concentration field, and the results are depicted by considering the presence and absence of chemical reaction. The variation of the Lewis number (Le) is presented within the range $1 \leq Le \leq 4$.

The Lewis number is a dimensionless quantity defined as the ratio of thermal diffusion to Brownian diffusion. Increasing the Lewis number signifies a significant enhancement in thermal diffusion and consequently a decrease in Brownian diffusion. This causes greater retardation in the concentration field, irrespective of the presence or absence of chemical reaction. Furthermore, the comparative analysis shows that the presence of chemical reaction also favors the control of fluid concentration throughout the flow domain. Therefore, the concentration boundary-layer thickness also decreases.

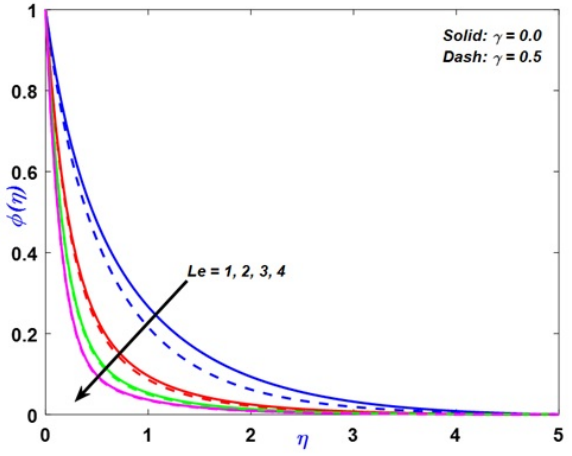

Figure 7. Impact of the Lewis number on the fluid concentration profile

Figures 8 and 9 indicate the variation of Brownian motion and thermophoresis on the solutal transport profile. As described earlier, with increasing Brownian motion, the diffusion of nanoparticles due to random

motion becomes more pronounced. This leads to a more uniform distribution of nanoparticles within the system in the steady-state case. However, higher values of Nb are significant in decelerating the solutal transfer profile. Furthermore, thermophoresis drives nanoparticles from hotter regions to cooler regions, and for increasing thermophoresis, this effect becomes stronger. This causes a significant enrichment in the fluid concentration, and higher values of Nt also enhance the profile significantly. In the unsteady-state case, the profile is enhanced in both cases, but Brownian motion is more pronounced in decelerating the profile, while thermophoresis enhances it throughout the flow domain.

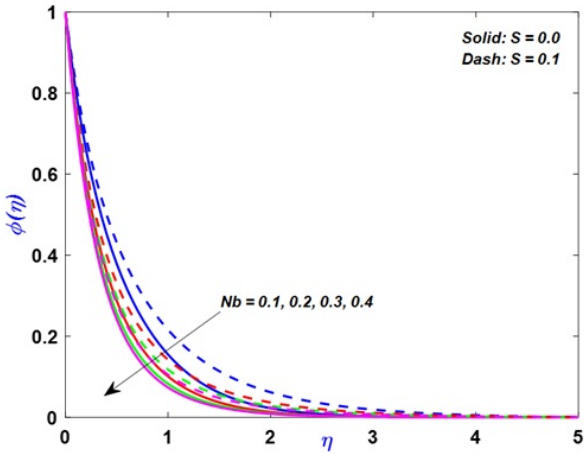

Figure 8. Behavior of Brownian motion on the fluid concentration profile

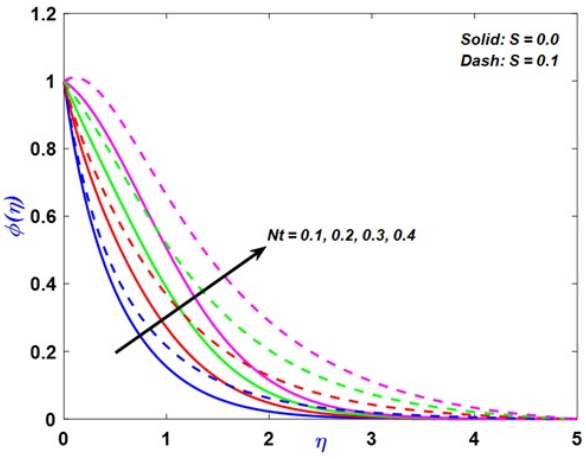

Figure 9. Role of thermophoresis on the concentration profile

4.4. Rate of heat and mass transfer profiles

The computation of the engineering coefficients for the variation of different parameters is also important, and these quantities are obtained numerically. The results for the shear rate in the form of the skin-friction coefficient or shear-drag rate coefficient, the heat transfer rate in the form of the Nusselt number, and the solutal transfer rate in the form of the Sherwood number are presented graphically.

Figure 10 portrays the behavior of magnetization, porosity, and the unsteadiness term on the skin-friction coefficient profile. The resistivity due to magnetization and porosity, which decelerates the velocity distribution, is significant in enhancing the velocity gradient with increasing values of these parameters. This causes an increase in the skin-friction coefficient for increasing magnetic and porosity parameters. Furthermore, enhanced unsteadiness also favors a significant increase in the skin-friction coefficient.

Figure 11 exhibits the variation of thermal radiation, Brownian motion, and thermophoresis on the heat transfer rate profile. The radiative heat energy is beneficial in increasing the heat transfer rate for its increasing

value. Therefore, the Nusselt number profile enhances with increasing thermal radiation. Furthermore, both Brownian motion and thermophoresis are significant in controlling the heat transfer rate, which causes retardation in the Nusselt number for increasing Brownian motion and thermophoresis parameters.

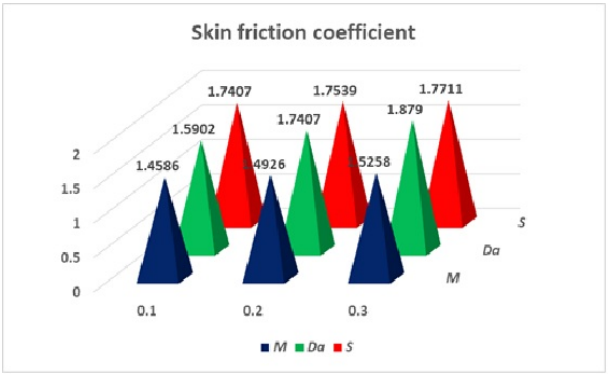

Figure 10. Role of various factors on the skin-friction coefficient

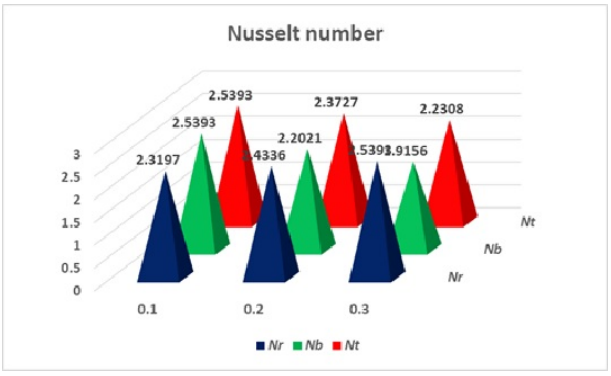

Figure 11. Role of various factors on the Nusselt number

Finally, Figure 12 displays the variation of the Lewis number and chemical reaction parameter on the solutal rate profile, represented by the Sherwood number. The graphical illustration, together with the corresponding numerical results, shows that increasing the Lewis number and chemical reaction parameter is significant in enhancing the Sherwood number at all points within the system.

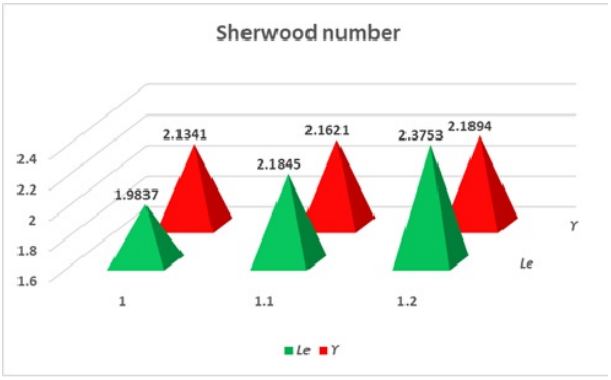

Figure 12. Role of various factors on the Sherwood number

5. Conclusion

The forced convection of a time-dependent electrically conducting nanofluid over an extending surface equipped with porous substances is analyzed in this article. The behavior of radiating energy, heat source/sink, and chemical species is accounted for in the flow phenomena, which enriches the physical model

significantly. A numerical treatment, namely the Runge–Kutta shooting technique, is adopted for the solution of the transformed flow phenomena, and the variations of the significant parameters are presented graphically. The important outcomes of the study are summarized as follows:

- The resistivity due to the inclusion of magnetization and porosity has greater control over the velocity profile, due to which the velocity profile retards.
- The enhanced stretching ratio is favorable in intensifying the fluid velocity, irrespective of the steady or unsteady state condition.
- The radiative heat interaction through thermal radiation enhances the thermal field effect.
- The collective impact of Brownian motion and thermophoresis favors the augmentation of the heat transfer phenomenon.
- The fluid concentration decelerates for enhanced Brownian motion, whereas a reverse impact is rendered for increasing thermophoresis.
- Both the Lewis number and the chemical reaction parameter have greater control over the fluid concentration, while the Sherwood number profile increases.

Although the present study provides a two-phase model for examining the impact of Brownian motion and thermophoresis on nanofluid flow with the involvement of several factors affecting the flow phenomena, it is necessary to enhance the study by introducing variable thermal conductivity and viscosity in future investigations. Therefore, the combination of the two-phase model and the Tiwari–Das model, generally called the modified model, may further enhance the heat transfer properties. Moreover, it may be beneficial to introduce a non-Newtonian model with hybrid nanofluid behavior, since enhanced thermal properties may be more effective in generating improved heat transfer rates.

Nomenclature

Symbol	Description
t	Time (s)
a, b	Stretching rate (s^{-1})
T_w	Wall temperature (K)
C_w	Wall concentration (kg m^{-3})
q_r	Radiative heat flux
Q	Internal heat source
K_p	Porous medium permeability (m^2)
α	Thermal diffusivity ($m^2 s^{-1}$)
τ	Specific heat capacity ratio
T_∞	Ambient temperature (K)
C_∞	Ambient concentration (kg m^{-3})
B_0	Magnetic field strength (Tesla)
σ^*	Stefan–Boltzmann constant (W m^{-2} K^{-4})
k^*	Mean absorption coefficient (m^{-1})
S	Transient parameter
Da	Porosity parameter
Nb	Brownian motion parameter
Nt	Thermophoresis parameter
Le	Lewis number
M	Magnetic parameter
γ	Chemical reaction parameter
C_f	Shear rate coefficient
Nu	Heat transfer rate
Sh	Solutal transfer rate
Re_x	Local Reynolds number

References

[1] Choi, S. U. (1995, November). Enhancing thermal conductivity of fluids with nanoparticles. In *ASME International Mechanical Engineering Congress and Exposition* (Vol. 17421, pp. 99-105). American Society of Mechanical Engineers.

[2] Mahian, O., Kianifar, A., Kalogirou, S. A., Pop, I., & Wongwises, S. (2013). A review of the applications of nanofluids in solar energy. *International Journal of Heat and Mass Transfer, 57*(2), 582-594.

[3] Buongiorno, J., Hu, L. W., Kim, S. J., Hannink, R., Truong, B. A. O., & Forrest, E. (2008). Nanofluids for enhanced economics and safety of nuclear reactors: an evaluation of the potential features, issues, and research gaps. *Nuclear Technology, 162*(1), 80-91.

[4] Saidur, R., Leong, K. Y., & Mohammed, H. A. (2011). A review on applications and challenges of nanofluids. *Renewable and Sustainable Energy Reviews, 15*(3), 1646-1668.

[5] Scherer, C., & Figueiredo Neto, A. M. (2005). Ferrofluids: properties and applications. *Brazilian Journal of Physics, 35*, 718-727.

[6] Murshed, S. M. S., Leong, K. C., & Yang, C. (2008). Thermophysical and electrokinetic properties of nanofluids–a critical review. *Applied Thermal Engineering, 28*(17-18), 2109-2125.

[7] Turkyilmazoglu, M. (2014). Nanofluid flow and heat transfer due to a rotating disk. *Computers & Fluids, 94*, 139-146.

[8] Hayat, T., Imtiaz, M., Alsaedi, A., & Alzahrani, F. (2016). Effects of homogeneous–heterogeneous reactions in flow of magnetite-Fe3O4 nanoparticles by a rotating disk. *Journal of Molecular Liquids, 216*, 845-855.

[9] Sheikholeslami, M. (2018). CuO-water nanofluid flow due to magnetic field inside a porous media considering Brownian motion. *Journal of Molecular Liquids, 249*, 921-929.

[10] Sheikholeslami, M. (2018). Numerical investigation for CuO-H2O nanofluid flow in a porous channel with magnetic field using mesoscopic method. *Journal of Molecular Liquids, 249*, 739-746.

[11] Sheikholeslami, M. (2018). Numerical investigation of nanofluid free convection under the influence of electric field in a porous enclosure. *Journal of Molecular Liquids, 249*, 1212-1221.

[12] Gorla, R. S. R., & Chamkha, A. (2013). Free convection past a vertical plate embedded in a porous medium saturated with a non-Newtonian nanofluid. *Journal of Nanofluids, 2*(4), 297-302.

[13] Gorla, R. S. R., & Chamkha, A. (2011). Natural convective boundary layer flow over a nonisothermal vertical plate embedded in a porous medium saturated with a nanofluid. *Nanoscale and Microscale Thermophysical Engineering, 15*(2), 81-94.

[14] Chamkha, J., Rashad, A. M., & Subba Reddy Gorla, R. (2014). Non-similar solutions for mixed convection along a wedge embedded in a porous medium saturated by a non-Newtonian nanofluid: natural convection dominated regime. *International Journal of Numerical Methods for Heat & Fluid Flow, 24*(7), 1471-1486.

[15] Chamkha, A., Abbasbandy, S., & Rashad, A. M. (2015). Non-Darcy natural convection flow for non-Newtonian nanofluid over cone saturated in porous medium with uniform heat and volume fraction fluxes. *International Journal of Numerical Methods for Heat & Fluid Flow, 25*(2), 422-437.

[16] Bég, O. A., Basir, M. F. M., Uddin, M. J., & Ismail, A. M. (2017). Numerical study of slip effects on unsteady asymmetric bioconvective nanofluid flow in a porous microchannel with an expanding/contracting upper wall using Buongiorno's model. *Journal of Mechanics in Medicine and Biology, 17*(03), 1750059.

[17] Li, J. J., Xu, H., Raees, A., & Zhao, Q. K. (2016). Unsteady mixed bioconvection flow of a nanofluid between two contracting or expanding rotating discs. *Zeitschrift für Naturforschung A, 71*(3), 261-272.

[18] Imtiaz, M., Hayat, T., Alsaedi, A., & Ahmad, B. (2016). Convective flow of carbon nanotubes between rotating stretchable disks with thermal radiation effects. *International Journal of Heat and Mass Transfer, 101*, 948-957.

[19] Hayat, T., Qayyum, S., Imtiaz, M., Alzahrani, F., & Alsaedi, A. (2016). Partial slip effect in flow of magnetite-Fe3O4 nanoparticles between rotating stretchable disks. *Journal of Magnetism and Magnetic Materials, 413*, 39-48.

[20] Bég, O. A., Rashidi, M. M., & Mehr, N. F. (2013). Second law analysis of hydromagnetic flow from a stretching rotating disk: DTM-Padé simulation of novel nuclear MHD propulsion systems. *Frontiers of Aerospace Engineering, 2*(1), 29-38.

[21] Hayat, T., Qayyum, S., Imtiaz, M., & Alsaedi, A. (2017). Radiative flow due to stretchable rotating disk with variable thickness. *Results in Physics, 7*, 156-165.

[22] Karimipour, A., Nezhad, A. H., D'Orazio, A., & Shirani, E. (2012). Investigation of the gravity effects on the mixed convection heat transfer in a microchannel using lattice Boltzmann method. *International Journal of Thermal Sciences, 54*, 142-152.

[23] Karimipour, A., Nezhad, A. H., D'Orazio, A., & Shirani, E. (2013). The effects of inclination angle and Prandtl number on the mixed convection in the inclined lid driven cavity using lattice Boltzmann method. *Journal of Theoretical and Applied Mechanics, 51*(2), 447-462.

[24] Karimipour, A., Nezhad, A. H., D'Orazio, A., Esfe, M. H., Safaei, M. R., & Shirani, E. (2015). Simulation of copper–water nanofluid in a microchannel in slip flow regime using the lattice Boltzmann method. *European Journal of Mechanics-B/Fluids, 49*, 89-99.

[25] Chamkha, A. J., & Aly, A. M. (2010). MHD free convection flow of a nanofluid past a vertical plate in the presence of heat generation or absorption effects. *Chemical Engineering Communications, 198*(3), 425-441.

[26] Biglarian, M., Gorji, M. R., Pourmehran, O., & Domairry, G. (2017). H2O based different nanofluids with unsteady condition and an external magnetic field on permeable channel heat transfer. *International Journal of Hydrogen Energy, 42*(34), 22005-22014.

[27] Rahimi-Gorji, M., Pourmehran, O., Gorji-Bandpy, M., & Ganji, D. D. (2016). Unsteady squeezing nanofluid simulation and investigation of its effect on important heat transfer parameters in presence of magnetic field. *Journal of the Taiwan Institute of Chemical Engineers, 67*, 467-475.

[28] Baag, S., & Mishra, S. R. (2015). Heat and mass transfer analysis on MHD 3-D water-based nanofluid. *Journal of Nanofluids, 4*(3), 352-361.

[29] Makinde, O. D., & Mishra, S. R. (2017). On stagnation point flow of variable viscosity nanofluids past a stretching surface with radiative heat. *International Journal of Applied and Computational Mathematics, 3*(2), 561-578.

[30] Das, K., Duari, P. R., & Kundu, P. K. (2014). Nanofluid flow over an unsteady stretching surface in presence of thermal radiation. *Alexandria Engineering Journal, 53*(3), 737-745.

[31] Baag, S., Mishra, S. R., Pattnaik, P. K., & Panda, S. (2024). Three-dimensional convective rotating hybrid nanofluid flow across the linear stretching/shrinking sheet due to the impact of dissipative heat. *Pramana, 98*(1), 21.

[32] Sahoo, R. K., Mishra, S. R., & Panda, S. (2024). Effective properties of binary chemical reaction with Brownian and thermophoresis on the radiative flow of nanofluid within an inclined heated channel. *Colloid and Polymer Science, 302*(9), 1337-1352.

[33] Panda, S., Baithalu, R., Baag, S., & Mishra, S. R. (2024). Behaviour of effective heat transfer rate in radiating micropolar nanofluid over an expanding sheet with slip effects. *Partial Differential Equations in Applied Mathematics, 11*, 100851.

[34] Li, S., Khan, M. I., Khan, S. U., Abdullaev, S., Mohamed, M. M. I., & Amjad, M. S. (2023). Effectiveness of melting phenomenon in two phase dusty carbon nanotubes (Nanomaterials) flow of Eyring-Powell fluid: Heat transfer analysis. *Chinese Journal of Physics, 86*, 160-169.

[35] Li, S., Rajashekhar, C., Nisar, K. S., Mebarek-Oudina, F., Vaidya, H., Khan, M. I., ... & Manjunatha, G. (2024). Peristaltic transport of a Ree-Eyring fluid with non-uniform complaint channel: An analysis through varying conditions. *ZAMM-Journal of Applied Mathematics and Mechanics/Zeitschrift für Angewandte Mathematik und Mechanik, 104*(2), e202300073.

[36] Li, S., Khan, M. I., Ali, F., Abdullaev, S. S., Saadaoui, S., & Habibullah. (2023). Mathematical modeling of mixed convective MHD Falkner-Skan squeezed Sutterby multiphase flow with non-Fourier heat flux theory and porosity. *Applied Mathematics and Mechanics, 44*(11), 2005-2018.

[37] Li, S., Abbas, T., Al-Khaled, K., Khan, S. U., Ul Haq, E., Abdullaev, S. S., & Khan, M. I. (2023). Insight into the heat transfer across the dynamics of Burger fluid due to stretching and buoyancy forces when thermal radiation and heat source are significant. *Pramana, 97*(4), 196.

[38] Sulochana, G., Prasad, C. V., Bhatti, S. K., Madhav, V. V., Saxena, K. K., Khan, M. I., ... & Khan, M. I. (2024). Impact of multi-walled carbon nanotubes (MWCNTs) on hybrid biodiesel blends for cleaner combustion in CI engines. *Energy, 303*, 131911.

[39] Li, S., Safdar, M., Taj, S., Bilal, M., Ahmed, S., Khan, M. I., ... & Abdullaev, S. S. (2023). Generalised Lie similarity transformations for the unsteady flow and heat transfer under the influence of internal heating and thermal radiation. *Pramana, 97*(4), 203.

[40] Li, S., Abbasi, A., Farooq, W., Gul, M., Khan, M. I., Nafasova, G., & Hejazi, H. A. (2025). Heat and mass transfer characteristics of Al2O3/H2O and (Al2O3+ Ag)/H2O nanofluids adjacent to a solid sphere: A theoretical study. *Numerical Heat Transfer, Part A: Applications, 86*(12), 3944-3962.

[41] Li, S., Khan, M. I., Ali, S., Ullah Khan, S., Althobaiti, S. A., Khan, I., ... & Kchaou, M. (2024). Influence of variable fluid properties on mixed convective Darcy–Forchheimer flow relation over a surface with Soret and Dufour spectacle. *Open Physics, 22*(1), 20240010.

[42] Ishak, A., Nazar, R., & Pop, I. (2009). Boundary layer flow and heat transfer over an unsteady stretching vertical surface. *Meccanica, 44*(4), 369-375.

[43] Vajravelu, K., Prasad, K. V., & Ng, C. O. (2013). Unsteady convective boundary layer flow of a viscous fluid at a vertical surface with variable fluid properties. *Nonlinear Analysis: Real World Applications, 14*(1), 455-464.

[44] Shamshuddin, M. D., Gamar, F., Salawu, S. O., & Reddy, B. P. (2025). Two-phase micropolar nanofluid flow in an isothermal extending porous sheet with heat radiation and chemical interaction: numerical study. *Partial Differential Equations in Applied Mathematics, 14*, 101226.

[45] Swapna, T., Salawu, S. O., Shamshuddin, M. D., & Sunder Ram, M. (2025). Nonorthogonal stagnation-point flow of micropolar fluid past a stretching sheet in the presence of thermal radiation and chemical reaction. *Heat Transfer, 54*(1), 1031-1051.

[46] Shamshuddin, M. D., Panda, S., Umavathi, J. C., Mishra, S. R., Alruwaili, A. S., & Eid, M. R. (2024). Diversified characteristics of the dissipative heat on the radiative micropolar hybrid nanofluid over a wedged surface: Gauss-Lobatto IIIA numerical approach. *Alexandria Engineering Journal, 106*, 448-459.

[47] Shamshuddin, M. D., Panda, S., Pattnaik, P. K., & Mishra, S. R. (2024). Ferromagnetic and ohmic effects on nanofluid flow via permeability rotative disk: significant interparticle radial and nanoparticle radius. *Physica Scripta, 99*(5), 055206.

[48] Sademaki, L. J., Shamshuddin, M. D., Salawu, S. O., & Reddy, B. P. (2024). Unsteady dynamical analysis of convective hydromagnetic thermal migration of chemically reacting tiny species with dissipation and radiation in an inclined porous plate. *International Journal of Modern Physics B, 38*(32), 2450442.

© 2026 by the authors; licensee PSRP, Lahore, Pakistan. This article is an open access article distributed under the terms and conditions of the Creative Commons Attribution (CC-BY) license (http://creativecommons.org/licenses/by/4.0/).